Journal of Physics: Conference Series **602** (2015) 012020 doi:10.1088/1742-6596/602/1/012020

FEM simulation of the size- and constraining effect in lead-free solder joints with the theory of strain gradient elasticity

M Lederer[1,2], J Magnien[1,2], G Khatibi[2] and B Weiss[2]
[1]Materials Center Leoben, Forschung GmbH, Roseggerstrasse 12, 8700 Leoben, Austria
[2]Faculty of Physics, University of Vienna, Boltzmanngasse 5, A-1090 Wien, Austria

E-mail: martin.lederer@univie.ac.at

Abstract. Reliability studies of electronic parts prevalently involve FEM simulations of solder joints under service conditions. However, simulations performed with classical continuum mechanics lead to strain singularities at the surface of material transitions. In consequence, the desired independence of the results from mesh size can usually not be achieved. Therefore, we propose a novel version of strain gradient elasticity which consequently removes strain singularities. Our approach shows similarities to a strain gradient theory which was developed already in the 1960s. But in our version of the theory it is required that the stress tensor of equilibrium states is always symmetric. This approach is implemented in the commercial FEM code ABAQUS through user subroutine UEL. Thus, it is demonstrated that in the new approach mesh convergence is achieved. Furthermore, simulations for solder joints of different sizes predict a mechanical size effect in the sense "smaller is stronger".

1. Introduction

The reliability of solder joints is a major issue of microelectronic industry. Lifetime models are usually based on Finite Element simulations revealing the stresses and strains observed in the constituent materials under service conditions. Due to the permanent miniaturization in microelectronics, the material properties of small scaled structures become increasingly important. It is well known that properties of materials in small dimensions cannot simply be deduced from the behaviour of bulk material. However, commercial Finite Element codes do not include a description of this size-effect. Moreover, the desired independence of the results from the mesh size can often not be achieved in the vicinity of material transitions at the sample surface. In order to solve these problems we propose a novel version of strain gradient elasticity which is implemented in the FEM code ABAQUS through user subroutine UEL. Approaching a microscopic length scale, the theory predicts a pronounced size-effect in the sense "smaller is stronger". Furthermore, mesh convergence is achieved by removal of stress singularities.

An earlier version of strain gradient elasticity [1, 2] was based on a publication of E & F Cosserat [3] who developed a theory of a three-dimensional continuous solid where every material point has six degrees of freedom. The additional degrees of freedom were microrotations which were considered supplementary to the displacements. The forces conjugated to microrotations were called couple stresses. This led to an enriched version of continuum mechanics which may for instance be applied to the propagation of acoustic waves in a crystal [4]. Within couple stress theory the stress tensor was

treated as asymmetric tensor. In equilibrium the torque arising from asymmetric stresses was compensated by the torque of couple stresses. Mindlin and Tiersten suggested [1] that couple stress theory may be utilized to evaluate size effects. They calculated the stress concentrations around spherical and cylindrical cavities in a field of simple tension. Thereby, it was found that the stress concentrations at small cavities were reduced in comparison to larger ones. Mindlin [2] related the microrotations to a bending of the microstructure. Further, the bending was related to a curvature which resulted from the strain gradient. In this way constitutive equations were obtained where the microrotations were no longer independent from the displacement field. Nevertheless, the stress tensor was still treated as asymmetric tensor. Sternberg and Muki [5] used this theory to calculate stress concentrations at the tip of a sharp crack. In fact, singularities were found for sharp cracks and similar geometries [6]. We here suggest a modification of this theory which leads to a removal of strain singularities.

2. A new version of strain gradient elasticity

We propose a theory of strain gradient elasticity which does not emerge from an enriched theory of continuum mechanics. This means that the degrees of freedom considered here are just the displacements. Rotations may only arise according to the polar decomposition of the deformation gradient tensor. In consequence, the stress tensor of our theory is symmetric in static equilibrium. Thus, the elastic energy writes as

$$W = \tfrac{1}{2} \int_V \left(\sigma_{ij} \varepsilon_{ij} + \mu_{ijk} \eta_{ijk} \right) dV \quad \text{with} \quad \mu_{ijk} = B\, \eta_{ijk}, \qquad (1)$$

where summation is carried out over repeated indices. The Cauchy stress σ_{ij} is related to the linear strain ε_{ij} by Hooke's law. η_{ijk} are the strain gradients $\partial^2 u_i / \partial x_j \partial x_k$, where u_i are the displacements and x_i are the coordinates. μ_{ijk} are higher order stresses related to strain gradients. The proportionality constant B is called bending modulus and has the dimension of a force. The existence of higher order stresses is explained by the fact that the correlated strain gradients lead to a bending of the crystal lattice. Since any perturbation of the lattice symmetry increases the energy of the system, stiffness against bending occurs. Our constitutive equation (1) represents the simplest approach of two-dimensional isotropic strain gradient elasticity. It should be noticed that this expression for the elastic energy fulfils the requirement of invariance with respect to rotation of the coordinate system.

3. Experimental results for the strain distributions observed in solder joints

Every material model developed for Finite Element simulations should be validated by comparison with experiments. However, there are some details where the agreement between theoretical predictions and test results cannot easily be achieved. A typical example is provided by specimens with a transition of materials at the sample surface.

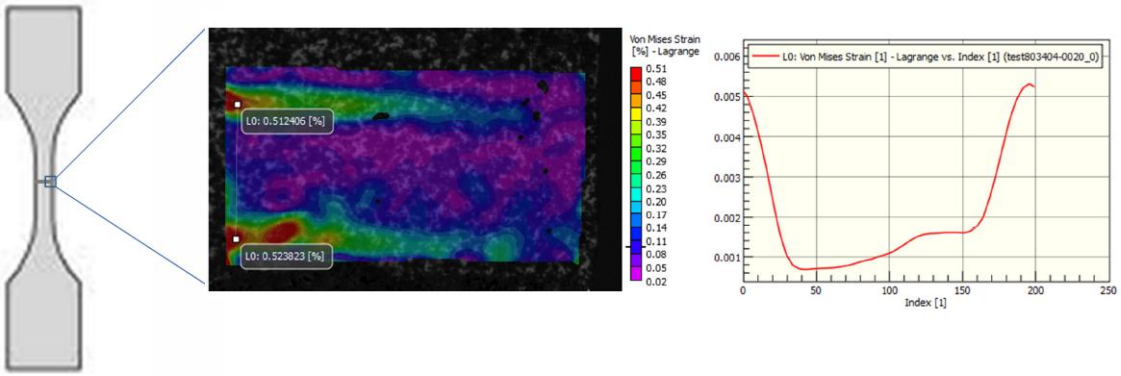

Figure 1. Schematic picture of the sample. Plot of the von Mises strain for a 404 µm thick solder gap at a tensile stress of 36.1 MPa.

In this case, the stress singularities predicted by classical continuum theory are not confirmed experimentally. In fact, the discrepancy between experiment and theory is not restricted to an infinitesimal region where the singularity should occur theoretically. Instead, deviations between model predictions and observed strain fields are also found in the neighbourhood of the critical region.

Tensile tests were performed with dumbbell shaped samples as depicted in figure 1, schematically. The specimens consisted of Sn-3.5Ag-0.7Cu solder gaps with cross sections of 3 x 2 mm^2 and pieces of 99.9% pure copper base material. The soldering process was carried out in a commercial reflow furnace using a suitable temperature profile. The samples were exposed to uniaxial tensile stress and the deformation of the solder joint was monitored with digital image correlation (DIC). The natural surface of the specimens provided a fine speckle pattern which was appropriate for high resolution DIC measurements. A plot of the von Mises strain showing the strain distribution of a 404 µm thick solder gap at a tensile stress of 36.1 MPa is shown in figure 1. The results of the contour plot along an indicated line between two points with white markings are displayed in the x-y plot on the right.

4. Finite Element Analysis

4.1 *Simulation with the classical continuum theory*

Three dimensional elasto-plastic simulations were performed for solder joints using cubic element shapes. Thereby, the element size was stepwise reduced. In consequence, the material transition between copper and solder led to the characteristics of a strain singularity within the solder material. At the beginning of mesh refinement the agreement between experiment (see figure 1) and simulation (see figure 2) improved until the best possible agreement was achieved. Thereafter, further mesh refinement deteriorated the results insofar as the strain maximum of the simulation exceeded the experimental values. Figure 2 shows two simulations performed with the material model of reference [7] using material parameters for Sn-3.5Ag-0.7Cu. Due to symmetry conditions, only $^1/_8$ of the sample was simulated. The element sizes used were (a) 28.86 µm and (b) 15.5 µm. In the latter case the mesh size was already too fine to capture the experimentally measured strain distribution at a tensile stress of 36.1 MPa:

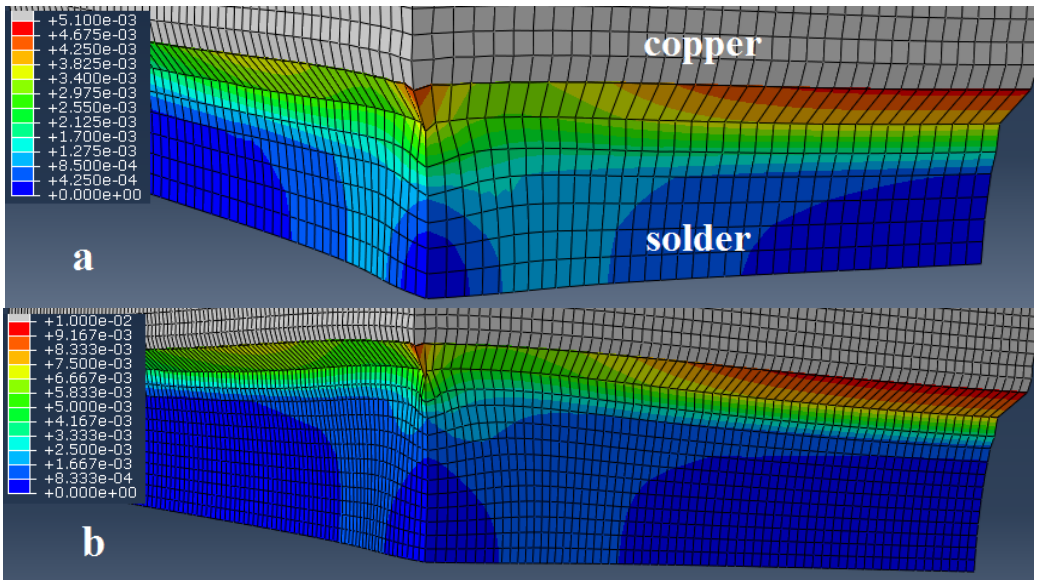

Figure 2. Plot of the plastic equivalent strain. Element size (a): 28.86 µm, (b): 15.5 µm

4.2 Implementation of strain gradient elasticity in ABAQUS

The theory of strain gradient elasticity defined in equation (1) is now implemented in the commercial software ABAQUS through user subroutine UEL. The elements used are 9-node squares consisting of isoparametric 4-node subelements as depicted in figure 3.

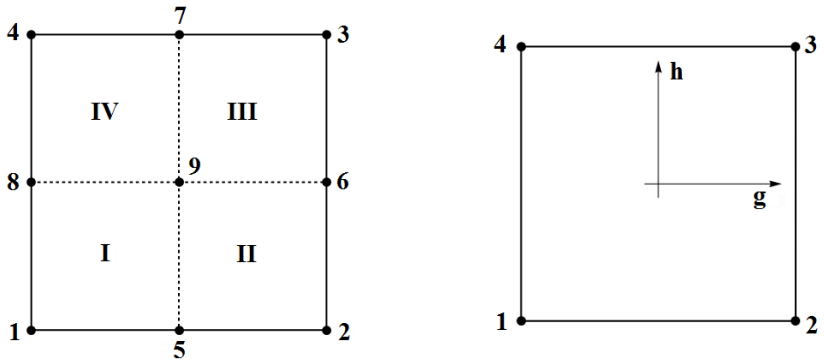

Figure 3. (a) left: 9-node elements consist of 4 node subelements which are indicated by italic numbers. (b) right: Subelements are isoparametric 4-node squares.

The interpolation functions for the displacements used on the subelement level are [8]:

$$U = ¼ (1–g)(1–h)U_1 + ¼ (1+g)(1–h)U_2 + ¼ (1+g)(1+h)U_3 + ¼ (1–g)(1+h)U_4 \qquad (2)$$

where g and h are the coordinates of the isoparametric space and U_1, U_2, U_3 and U_4 are the displacement vectors of the nodes 1, 2, 3, and 4, respectively. The strains are calculated at integration points which are located in the middle of the subelements. Further, the strain gradients $\eta_{112} = \eta_{121}$ and $\eta_{212} = \eta_{221}$ are obtained by differentiating the interpolation functions for the displacements in the global coordinate system twice at the integration points. However, the strain gradients η_{111}, η_{122}, η_{211} and η_{222} may not adequately be determined within subelements. Instead, they are derived at the level of the entire element by comparison of the strain components of neighbouring subelements.

Next, the residual nodal forces related to stresses and higher order stresses are applied according to the principle of superposition. Higher order stresses are always counteracting the deformation introduced by the corresponding strain gradients. The directions of the nodal forces are illustrated in figure 4. The values of nodal forces are obtained by the condition that the work done by external forces equals the elastic energy stored in the element. In the case of $\eta_{112} = \eta_{121}$ this leads to the equation

$$F_{1,x} = – F_{2,x} = F_{3,x} = – F_{4,x} = – B\,\eta_{112} – B\,\eta_{121} \qquad (3)$$

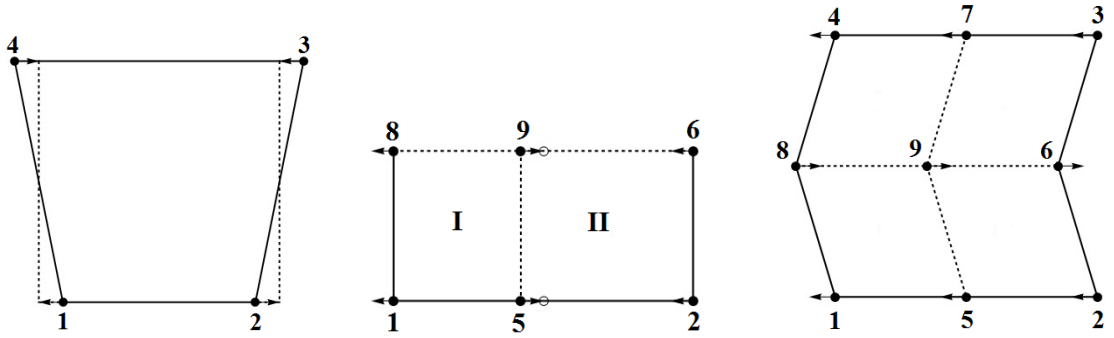

Figure 4. Directions of residual nodal forces. (a) left: $\eta_{112} = \eta_{121}$, (b) middle: η_{111} and (c) right: η_{122}.

The case of $\eta_{212} = \eta_{221}$ is analogous to $\eta_{112} = \eta_{121}$. Further, one gets for η_{111}

$$F_{1,x} = F_{2,x} = – B\,\eta_{111}^{(12)}, \qquad F_{3,x} = F_{4,x} = – B\,\eta_{111}^{(34)},$$
$$F_{5,x} = 2\ B\,\eta_{111}^{(12)}, \qquad F_{6,x} = F_{8,x} = – B\,(\eta_{111}^{(12)} + \eta_{111}^{(34)}),$$
$$F_{7,x} = 2\,B\,\eta_{111}^{(34)} \quad \text{and} \quad F_{9,x} = 2\,B\,(\eta_{111}^{(12)} + \eta_{111}^{(34)}), \qquad (4)$$

where the superscript (ij) indicates that this gradient was obtained by comparison of subelements i and j. The case of η_{222} is analogous to η_{111}. Further, one obtains for η_{122}:

$$F_{1,x} = F_{4,x} = -B\,\eta_{122}^{(14)}, \qquad F_{2,x} = F_{3,x} = -B\,\eta_{122}^{(23)},$$
$$F_{5,x} = F_{7,x} = -B\,(\eta_{122}^{(14)} + \eta_{122}^{(23)}), \qquad F_{6,x} = 2B\,\eta_{122}^{(23)},$$
$$F_{8,x} = 2B\,\eta_{122}^{(14)} \text{ and} \qquad F_{9,x} = 2B\,(\eta_{122}^{(14)} + \eta_{122}^{(23)}). \qquad (5)$$

The case of η_{211} is again analogous.

In strain gradient elasticity, it is necessary to fulfil boundary conditions for the strains at the borders of neighbouring elements. This problem is solved here with an overlapping mesh technique as illustrated in figure 5.

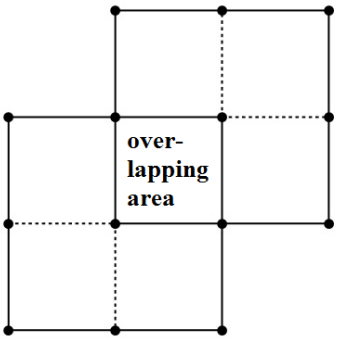

Figure 5. Boundary conditions for strains are solved with use of an overlapping mesh technique.

This mesh technique involves the definition of 6-node elements at the sample boundary. In addition, also symmetry elements were defined by assuming virtual nodes which are mirrored at symmetry lines. Since the whole sample is meshed twice, the values for Young's modulus and bending modulus are halved at the element level in order to get the right values for the complete model. The main advantage of the overlapping mesh technique compared to other methods satisfying strain boundary conditions is that we obtain a linear system of equations which may be solved precisely.

4.3. Simulation of solder joints with strain gradient elasticity

In order to prove mesh convergence, we first apply the theory to a simplified model of a solder joint where only the solder material is deformable while the base material is treated as rigid solid. A sketch of the sample and the boundary conditions may be seen in figure 6 (a). The sketch represents ¼ of a sample with 1.5 mm length and 100 µm thickness. The upper line of the model is fully constrained while the bottom line is shifted 20 nm downwards. At the left side of the model and along the bottom line symmetry conditions were applied. Figures 6 (b) and (c) show that the contour plots for the von Mises stress [MPa] are nearly independent of the mesh size. For the simulations, a bending modulus of B = 7.416 N was assumed.

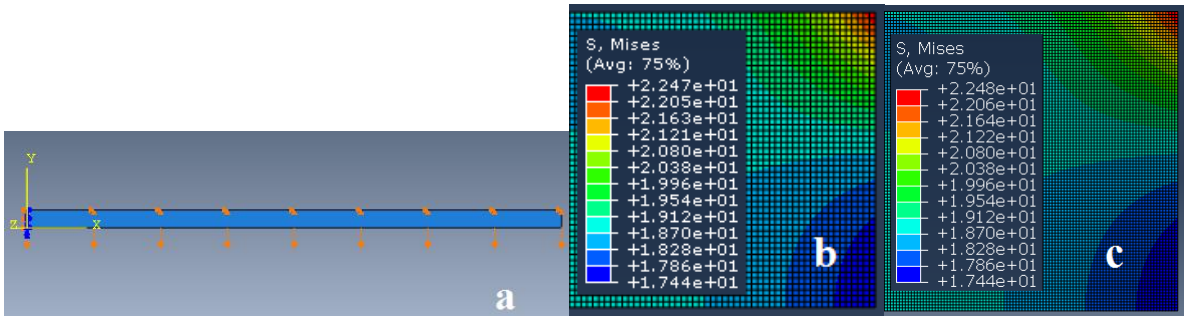

Figure 6. (a) sketch of sample and boundary conditions. (b) right sample end, subelement mesh size of 1 µm. (c) subelement mesh size of 0.5 µm.

Figure 7 shows a more realistic model of a solder joint where solder and base material were both simulated as deformable bodies. The comparison of figures 7 (a) and (b) with solder gap dimensions of 1.5 x 0.4 mm^2 and 0.75 x 0.2 mm^2, respectively, demonstrates the influence of the size effect in the sense "smaller is stronger". In both cases the average strain along the tensile direction was the same, but the maximum of von Mises stress [MPa] at the material transition is reduced for the smaller sample. Therefore, the smaller sample is expected to carry higher tensile stresses when loaded until fracture. In the simulations it was assumed that the bending moduli of copper and solder are proportional to the Young's moduli of these materials.

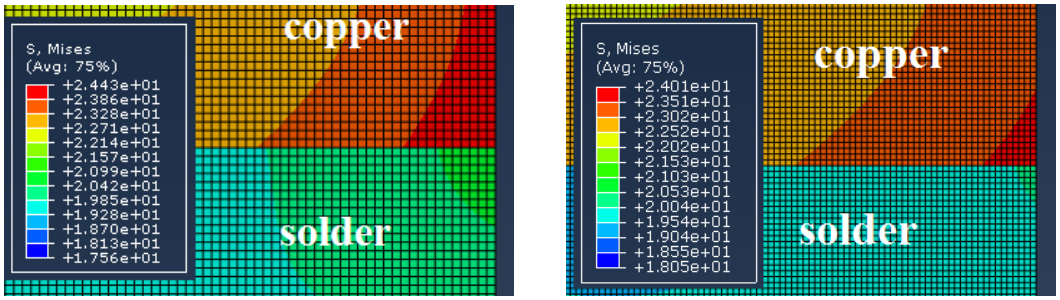

Figure 7. Samples with dimensions of 1.5 x 0.4 mm^2 (left) and 0.75 x 0.2 mm^2 (right), respectively. The material transition at the surface is shown in magnification.

5. Summary and conclusions

The modelling of solder joints within classical continuum mechanics leads to a strain singularity at the surface of a material transition. In consequence, the simulation results are not independent from the mesh size. This problem was solved with strain gradient theory. Our approach of strain gradient elasticity is similar to a theory proposed by Mindlin in the 1960s. However, we require that the stress tensor of static equilibrium must be symmetric. In consequence, the strain singularity at the surface of the material transition was removed and independence of the results from the mesh size could be achieved. Moreover, the theory predicts a size effect in the sense "smaller is stronger". Future work on this topic shall include 3-dimensionality, plasticity and time dependent behaviour.

Acknowledgments

Financial support by the Austrian Federal Government (in particular from Bundesministerium für Verkehr, Innovation und Technologie and Bundesministerium für Wirtschaft, Familie und Jugend) represented by Österreichische Forschungsförderungsgesellschaft mbH and the Styrian and the Tyrolean Provincial Government, represented by Steirische Wirtschaftsförderungsgesellschaft mbH and Standortagentur Tirol, within the framework of the COMET Funding Programme is gratefully acknowledged.

6. References

[1] Mindlin R D and Tiersten H 1962 *Arch. Rat. Mech. Anal.* **11** 415
[2] Mindlin R D 1963 *Experimental Mechanics* **3** 1
[3] Cosserat E, Cosserat F 1909 *Théorie des corps dé formables*, Librairie Scientifique A. Hermann et Fils, Paris. (English trans. by Delphenich D, 2007. Theory of deformable bodies.)
[4] Aero E L and Kuvshinskii E V 1961 *Soviet Physics Solid State* **2** 1272
[5] Sternberg E and Muki R 1967 *Int. J. Solids Structures* **3** 69
[6] Muki R and Sternberg E 1965 *Z. angew. Math. Phys.* **16** 611
[7] Lederer M, Khatibi G and Weiss B 2012 *Int. J. Solids Structures* **49** 3453
[8] Bathe K J 2006 *Finite Element Procedures*, Prentice Hall, Pearson Education Inc.